Exploiting the Spatio-Temporal Coherence of Ocean Ambient Noise for Passive Tomography.

Karim G. Sabra,
School of Mechanical Engineering, Georgia Institute of Technology
Atlanta, GA 30332
Phone: (404) 385-6193 Fax(404) 894-1658 E-mail: karim.sabra@me.gatech.edu

Award number: **N000141110050**

LONG TERM GOALS

To develop passive modalities of acoustic ocean monitoring techniques such as acoustic tomography or acoustic thermometry using Cross-correlation processing of ocean ambient noise

OBJECTIVE

Coherent processing of ambient noise, based on these computed noise cross-correlation between receivers, has been suggested as a potential means for developing passive methods for ocean acoustic tomography or thermometry [Roux et al., 2004]. However, this technique can require long recording times to extract stable coherent arrivals from ocean noise correlations [Sabra et al., 2005a; Godin, 2010]. Array beamforming can enhance the emergence of such deterministic arrivals between receiver arrays. For instance, a single vertical array was used to improve passive imaging of seabed layers [Siderius et al., 2010; Siderius, 2011; Traer and Gerstoft, 2011].

The main objective of this year research was to develop a general spatiotemporal filtering (STF) technique to enhance the emergence rate of coherent wavefronts between two spatially separated receiver arrays. The performance of this STF technique was demonstrated using ocean ambient noise recordings dominated by non-stationary shipping noise to monitor the arrival-time fluctuations of coherent noise wavefronts over a six day long observation time.

WORK COMPLETED

Ambient noise was recorded on two vertical line arrays (VLAs) separated by 450 m and deployed in shallow water (depth ~150 m) off San Diego, CA continuously for six days. Recordings were dominated by non-stationary and non-uniform broadband shipping noise (250 Hz-1.5 kHz). Stable coherent noise wavefronts were extracted from ambient noise correlations between the VLAs during all six days by mitigating the effect of discrete shipping events and using array beamforming with data-derived steering vectors. This procedure allows the tracking of arrival-time variations of these coherent wavefronts during six days and may help developing future passive acoustic tomography systems. A detailed summary of the completed work is provided hereafter.

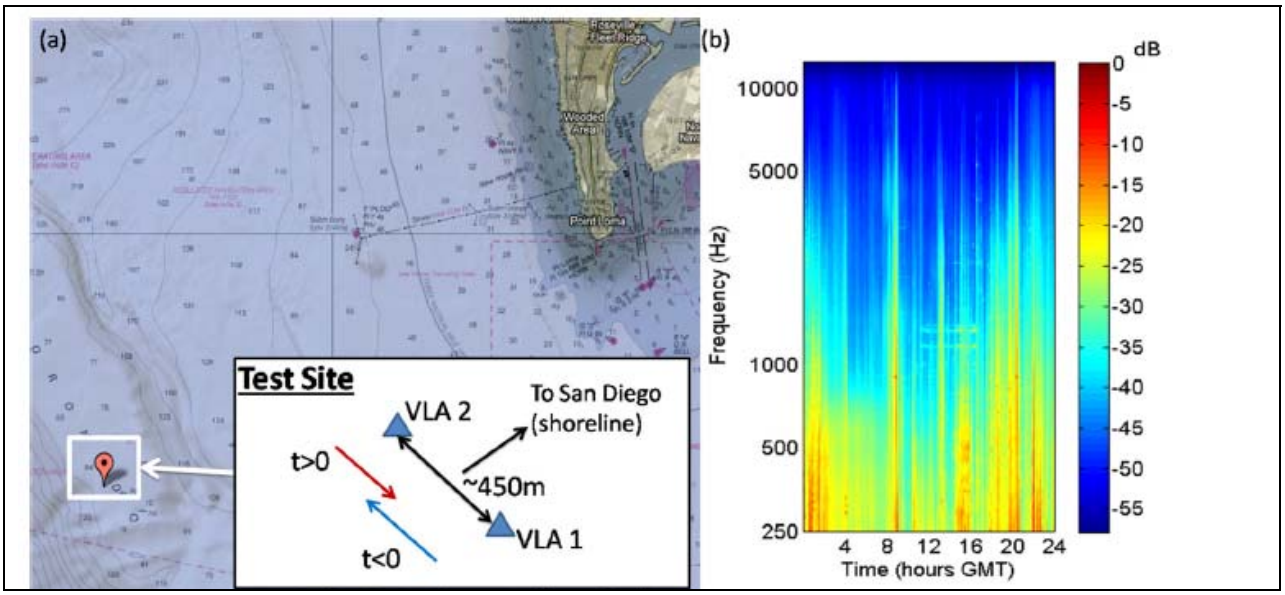

Fig. 1 (a) Bathymetry map (depth denoted in fathoms) in the vicinity of the harbor of San Diego, CA. The test site, marked by a box, is located on the shallow Coronado Bank (water depth ~150m). The zoomed-in inset in the bottom-right corner sketches the relative orientation of the two VLAs with respect to the shoreline. (b) Averaged spectrogram of the ambient noise (across the all 16 elements of VLA1) recorded on the third day of the experiment in the frequency band [250 Hz–12.5 kHz]. The vertical axis represents the acoustic frequency in a logarithmic scale. The horizontal axis indicates Greenwich Mean Time.

Broadband ambient noise [250 Hz–12.5 kHz] was recorded continuously for six days from January 31 to February 5, 2009 (denoted as Days 1-6) near San Diego, CA using two identical VLAs moored 450 m apart in a shallow and nearly range-independent section of the Coronado Bank (water depth ~150 m, Fig. 1(a)). Each VLA had 16 elements uniformly spaced by 1 m; the first element being ~7 m above the seafloor. Other technical features of the hydrophone array deployment and the electronic system have been described previously [Skinner et al., 2008; Leroy et al., 2012].

Due to the proximity of San Diego's harbor, acoustic data were dominated by non-stationary shipping noise, with episodic loud discrete shipping events, for frequencies below 2 kHz (see Fig. 1(b)). In order to mitigate the effects of these episodic shipping events, the continuous noise recordings from each hydrophone were segmented in 1 minute long intervals and then homogenized using the same two processing steps described in previous studies [Sabra et al., 2005b; Leroy et al., 2012]: (1) whitening the amplitude spectrum of the data in the most energetic frequency band [250 Hz - 1.5 kHz] to diminish eventual strong spectral peaks and (2) clipping the signal amplitudes above a threshold equal to three times the average standard deviation of the frequency whitened time series.

3. Spatial origin of the coherent noise field

Given each 1 minute long frequency-whitened and clipped time-series $S_i^{(1)}(t;k)$ and $S_j^{(2)}(t;k)$ recorded respectively by the ith and jth hydrophone of VLA1 and VLA2 (i,j=1..16) during the kth minute of the six day long recording (k=1..8640), their normalized cross-correlation function $C_{i,j}(t;k)$ was computed using:

$$C_{ij}(t;k) = \int S_i^{(1)}(\tau;k) S_j^{(2)}(\tau+t;k) d\tau \Big/ \sqrt{\int (S_i^{(1)}(\tau;k))^2 \, d\tau} \sqrt{\int (S_j^{(2)}(\tau;k))^2 \, d\tau} \qquad (1)$$

Subsequently, the ensemble averaged cross-correlation waveform $R_{i,j}(t;L,N)$ is defined hereafter over a N minute long recording interval starting at the L[th] minute of the six day long recording,

$$R_{i,j}(t;L,N) = \frac{1}{N}\sum_{k=L}^{L+N} C_{i,j}(t;k) \tag{2}$$

Fig. 2(a-d) displays the coherent wavefronts extracted from the ensemble averaged cross-correlation $R_{i,j}(t;L,N)$ over a 32 hour long interval (i.e. N=1920) starting on either the third day (L=2881) or fifth day (L=5761) of the experiment for both positive and negative time-delays. Based on Eq. (1), the main coherent wavefront in Fig. 2(c-d), centered on the negative time-delay t= -0.3 s (consistent with the VLAs separation of ~450 m) results from coherent ambient noise propagating successively between VLA1 and VLA2 (i.e. along the northward direction, see inset on Fig. 1(a)) for Day 3 or Day 5. Furthermore, the similarity of the arrival-times of these coherent wavefronts obtained (Fig. 2(c-d)) is indicative of the relative stability of the water column between the VLAs (especially at depths below 138 m) during this experiment between Day 3 and Day 5. Conversely, coherent wavefronts occurring at positive time delays correspond to coherent ambient noise propagating successively between VLA2 and VLA1 in the southward direction (Fig. 2(a-b)). Due to the proximity of the main shipping lanes exiting San Diego's harbor just north of the experimental site (see Fig. 1(a)), it was found that these coherent wavefronts for positive time-delays were more dominated by isolated loud shipping events while the coherent wavefronts for negative time-delays resulted from more diffuse shipping noise. This explains the slightly different wavefront structures and time delays of the positive arrival wavefronts (Fig. 2(a-b)) when compared to the negative arrival wavefronts (Fig. 2(c-d)). For instance, the coherent wavefronts shown on Fig. 2(b) were likely dominated by a single loud shipping event passing close to the VLAs and thus generating a more complex multipath structure when compared to Fig. 2(c-d).

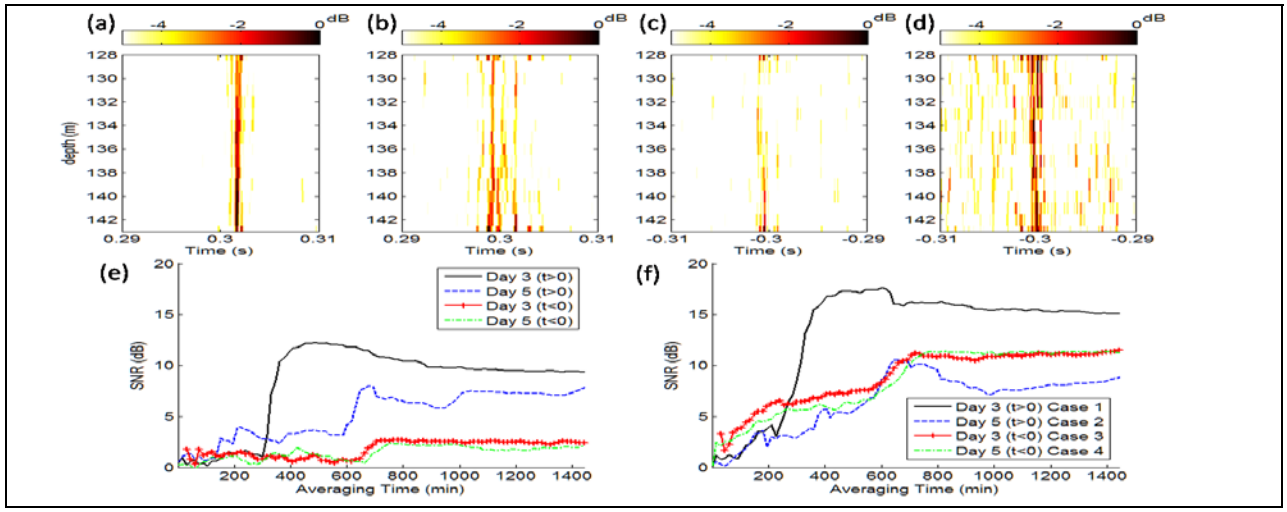

Fig. 2 *Spatial temporal representation (in logarithmic scale) of the coherent wavefronts obtained from the ensemble averaged cross-correlation* $R_{i,j}(t;L,N)$ *(see Eq. (2)) between hydrophone i=4 of VLA1 and all receivers of VLA2 (plotted by associated depth), for a 32 hour (i.e. N=1920) long recording interval starting at the first minute of each respective day; (a) Day 3 positive arrivals, (b) Day 5 positive arrivals, (c) Day 3 negative arrivals, and (d) Day 5 negative arrivals. The maximum value in each plot was set to unity (i.e., 0 dB).* ***(e)*** *Comparison of the evolution of the peak SNR (see Eq. (3)) of the*

ensemble averaged correlation waveform $R_{i=4,j=2}(t;L,N)$ *computed between an arbitrary selected pair of hydrophones of the VLAs for increasing averaging time (N=1…1440) starting from either the first minute of Day 3 or Day 5. The evolution of the peak SNR is computed for positive and negative time-delays in the same time windows around the arrivals as shown on* ***(a-d)****.* ***(f)*** *Same as* ***(e)*** *using instead the peak SNR of the beamformer output* $B(t,L,N)$ *. The four sets of coherent wavefronts shown in* ***(a-d)*** *were to determine the four different sets of steering vectors used to compute the beamformer output* $B(t,L,N)$ *for each case.*

4. Arrival-times variations of coherent noise wavefronts

A coherent arrival is clearly visible on the averaged cross-correlation waveform $R_{i,j}(t;L,N)$ only when this arrival's amplitude (the signal of interest, e.g. see coherent wavefront on Fig. 2(a)) becomes larger than the peak amplitude of the residual temporal fluctuations (which sets the background "noise" level of this waveform) in $R_{i,j}(t;L,N)$ occurring around the coherent arrival time |t|~0.3 s. Assuming that these residual temporal fluctuations behave as Gaussian random signals, their peak amplitude can be estimated by three times the standard deviation of $R_{i,j}(t;L,N)$ [Bendat and Piersol, 2000]. Hence, the peak signal-to-noise ratio $SNR(L,N)$ of the averaged cross-correlation waveform $R_{i,j}(t;L,N)$ is defined as:

$$SNR(L,N) = 10\log_{10}\left(\max_{t\in Tw}\left(\frac{R_{i,j}(t;L,N)}{3\sqrt{\frac{1}{N}\left(\frac{1}{N}\sum_{k=L}^{L+N}(C_{i,j}(t;k))^2-\left(\frac{1}{N}\sum_{k=L}^{L+N}C_{i,j}(t;k)\right)^2\right)}}\right)\right) \quad (3)$$

where the maximum amplitude search is performed in a 20 ms long time window T_w centered on the expected arrival time |t|~0.3 s of the main coherent wavefronts (see Fig. 2). The denominator in Eq. (3) represents three times the standard deviation of the ensemble averaged correlation $R_{i,j}(t;L,N)$ assuming that the fluctuations amongst the individual cross-correlation functions $C_{i,j}(t;k)$ are uncorrelated and have the same standard deviation [Weaver and Lobkis, 2005].

Fig. 2(e) compares the evolution of this peak value of $SNR(L,N)$ for both positive and negative time delays for increasing averaging duration up to 24 hrs (1≤N≤1440) using noise data recorded on either the third (L=2881) or fifth (L=5761) day of the experiment between the fourth element of VLA1 and the second element of VLA2 (i=4,j=2). Note that none of the peak SNR curves increases proportionally to the theoretical predictions of $\sqrt{N}$ derived for a stationary and isotropic ambient noise field [Sabra et al., 2005b; Weaver and Lobkis, 2005]. Indeed, the peak SNR for both negative and positive time-delays builds up non-uniformly primarily due to the occurrence of loud shipping events; especially around N=300-460 min on Day 3 for positive time delays (solid and dashed lines) or around N=650-750 min on Days 3 and 5 for negative time delays (plus and dot-dash lines). Additionally, the peak SNR remains low (<5 dB) even with long averaging times for negative time-delays.

In order to enhance the emergence rate of coherent wavefronts across all six days of the experiment, the STF methodology introduced by Leroy et al. (2012) was implemented to beamform the averaged cross-correlation waveforms $R_{i,j}(t;L,N)$ (i,j=1…M=16). At the frequency *f*, the beamformer output

$\hat{B}(f,L,N)$ corresponding to the Mx1 steering vectors $W_1(f)$ and $W_2(f)$ applied respectively to the M=16 elements of VLA1 and VLA2 is given by:

$$\hat{B}(f,L,N) = W_1{}^H(f)\,\hat{\mathbf{R}}(f,L,N)\,W_2(f) \tag{4}$$

where the superscript ^{H} denotes a complex transpose operation and $\hat{\mathbf{R}}(f;L,N)$ is the MxM cross-covariance matrix between VLA1 and VLA2. The (i,j)th entry of the matrix $\hat{\mathbf{R}}(f;L,N)$ is the Fourier transform of averaged cross-correlation waveforms $R_{i,j}(t;L,N)$ at the frequency *f*. In order to assess the performance of the STF methodology, the steering vectors $W_1(f)$ and $W_2(f)$ were computed hereafter for four different cases. As suggested by Leroy et al. (2012), the steering vectors $W_1(f)$ and $W_2(f)$ for Cases 1-4 were set as the first left and right singular vectors of four different reference covariance matrices $\hat{\mathbf{R}}_{ref}(f;L,N)$ corresponding to the four sets of coherent wavefronts shown on Fig. 2(a-d). Each reference is a 32 hour long average (N=1920), which starts on Day 3 (L=2881) or Day 5 (L=5761) for positive arrivals (Case 1 and Case 2) or for negative arrivals (Case 3 and Case 4).

The cross-correlation of time domain beamforming on VLA1 and VLA2, $B(t,L,N)$ was obtained from the inverse Fourier transform of the beamformer $\hat{B}(f,L,N)$ computed with Eq. (4) using each of the four sets of steering vectors $W_1(f)$ and $W_2(f)$ defined above (Cases 1-4). The SNR of the peak arrival of $B(t,L,N)$ was defined in a similar fashion to Eq. (3). Overall, compared to the results for the element-to-element correlations shown in Fig. 2(e), Fig. 2(f) indicates the peak SNR of the beamformer $B(t,L,N)$ grows more rapidly and more uniformly during the same 24 hour averaging interval. For instance, the peak SNR of the beamformer exceeded an arbitrary threshold of 5 dB using an N=480 min (i.e. 8 hrs) recording window for Cases (1-4).

Finally, the four different sets of steering vectors (Cases 1-4) were successively applied to the entire six day long dataset to beamform all cross-covariance matrices $\hat{\mathbf{R}}(f;L,N=480)$ ($1 \le L \le 8160$) computed using a short moving average of N=480 min. Fig. 3 displays the time shifts of the peak coherent arrival of the corresponding beamformer $B(t,L,N=480)$ (for Cases 1-4) vs. indices L (i.e. the beginning of the moving time-window along the "Slow Time" axis) when the peak SNR was sufficiently high (i.e. here above an arbitrary threshold of 1.5 dB) to ensure clear arrival tracking. Overall, this STF technique was robust enough to extract a small and quasi-linear upward trend of the peak coherent arrival of the beamformer $B(t,L,N=480)$ during the entire six days of the experiment for all four different sets of steering vectors (see Fig. 3). A comparison between the positive arrivals Fig. 3(a-b) and the negative arrivals Fig. 3(c-d) shows that Cases 3-4 have smoother and more consistent arrival tracking. This difference is likely due to the varying spatial and temporal features of the noise field generating these coherent wavefronts (i.e. individual loud ship events for positive arrivals versus more diffuse shipping noise for negative arrivals). Furthermore, as expected, the peak SNR is highest around the specific day or time interval that is used to construct each of the reference covariance matrices $\hat{\mathbf{R}}_{ref}(f;L,N)$ as marked on the horizontal axis of Fig. 3 with a red line. This suggests that updating the reference covariance matrices $\hat{\mathbf{R}}_{ref}(f;L,N)$ during the span of the total observation period may enhance the robustness of the STF technique for noise-based ocean monitoring (e.g. by using a different reference covariance matrices for each day of the experiment).

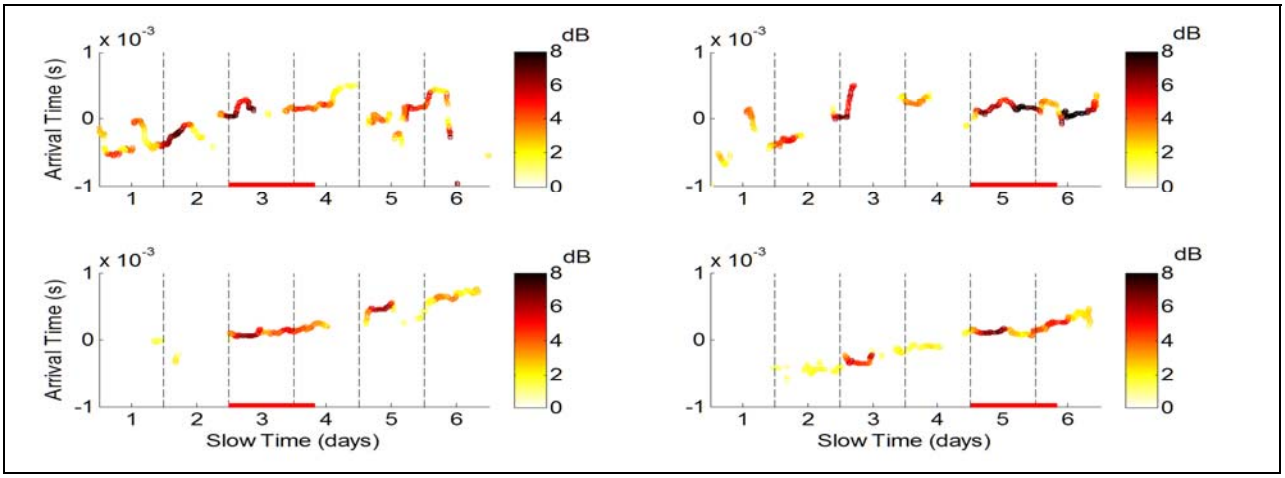

Fig. 3 *Variations of the arrival time of the peak coherent arrival of the beamformer* $B(t, L, N = 480)$ *over 6 days for four different sets of steering vectors* ***(a-d)*** *which were selected from the same Cases 1-4 used in Fig. 2(f). The beamformer output was computed for the ensemble averaged cross-correlation waveforms between both VLAs obtained using a short moving average of N=480 min starting at successive minutes L over 6 days (i.e. 1≤L≤8160). The index L thus represents the beginning of the moving time-window along the "Slow Time" axis.*

The total cumulated time shift over 6 days was found to be positive for Cases 1-4, and the shifts amounted respectively to +1.1 ms, +0.7 ms, +1.1 ms, and +1.1 ms (see Fig. 4(a-d)). Note that the cumulated time shift has the *same* sign (positive) when tracking coherent wavefronts occurring at positive time-delays (Cases 1-2) or negative-time delays (Cases 3-4). Thus, this time shift corresponds to an asymmetric (or non-reciprocal) change in arrival times when comparing positive and negative coherent wavefronts. Hence, this overall asymmetric time-shift is likely dominated by a relative clock drift of ~200 μs/day between the VLAs autonomous recording systems (which causes an imperfect synchronization of the noise records) as its trend is quasi-linear over six days and most likely not from an actual ocean current flowing between the VLAs [Sabra et al., 2005b]. Furthermore, other environmental causes (e.g. variations in the ocean sound speed or separation distance between the VLAs) would have otherwise caused symmetric (or reciprocal) time-shifts of opposite signs with respect to t=0 for positive and negative coherent wavefronts [Sabra et al., 2005b].

CONCLUSIONS

The results of this research effort confirm the possibility of tracking small fluctuations of deterministic coherent noise arrivals between acoustic arrays in a challenging coastal environment dominated by non-stationary and non-uniform shipping noise. Further studies are required to fully assess the potential of noise-based ocean monitoring and tomography over very long observation periods and larger array separation distances.

IMPACT

It is conjectured that the results of this study could help develop a totally passive means for monitoring the ocean environment using only ambient noise. A potential scenario benefiting from the proposed methodology might include long-term deployment of ocean sensing systems requiring minimum power

consumption, covert operations in hostile settings, or coastal deployments where active sources are limited by environmental regulations.

PUBLICATIONS

S. Lani, K.G. Sabra, W.S. Hodgkiss, W.A Kuperman, and P. Roux, “Coherent processing of shipping noise for ocean monitoring” J. Acoustical Society of America, 133, EL108-EL113 (2013).

REFERENCES

Bendat, J. S., and Piersol, A. G., (2000) *Random Data: Analysis & Measurement Procedures* pp. 272-286, 358 (Wiley-Interscience).

Godin, O., Zabotin, N., and Goncharov, V. (2010). "Ocean tomography with acoustic daylight," Geophys. Res. Lett. 37, L13605.

Leroy, C., Lani, S., Sabra, K. G., Hodgkiss, W., Kuperman, W. A., Walker, S., Roux, P. (2012). "Enhancing the emergence rate of coherent wavefronts from ambient shipping noise correlations using spatio-temporal filters," J. Acoust. Soc. Am. 132, 883-893.

Roux, P., Kuperman, W. A., and the NPAL Group, (2004). "Extracting coherent wavefronts from acoustic ambient noise in the ocean," J. Acoust. Soc. Am. 116, 1995-2003.

Sabra, K. G., Roux, P., and Kuperman, W. A. (2005a). "Emergence rate of the time-domain Green's function from the ambient noise cross-correlation function," J. Acoust. Soc. Am. 118, 3524-3531.

Sabra, K.G., Roux, P., Thode, A., D’Spain, G. L., Hodgkiss, W. S. and Kuperman, W. A., (2005b) “Using ocean ambient noise for array element self-localization and self-synchronization,” *IEEE J. Oceanic Engineering*. 30 (2), 338- 347.

Siderius, M., (2011). "Using practical supergain for passive imaging with noise," J. Acoust. Soc. Am. 131, EL14-EL20

Siderius, M., Song, H., Gerstoft, P., Hodgkiss, W., Hursky, P., and Harrison, C. (2010). "Adaptive passive fathometer processing," J. Acoust. Soc. Am. 127, 2193-2200.

Skinner, J. D. and Hodgkiss, W. S. (2008). "A networked/autonomous receiving array system," in Proceedings of the OCEANS 2008, IEEE, Quebec City.

Traer, J., and Gerstoft, P., (2011). "Coherent averaging of the passive fathometer response using short correlation time," J Acoust. Soc. Am. 130, 3633-3641.

Weaver, R. L. and Lobkis, O. I. (2005). "The mean and variance of diffuse field correlations in finite bodies," J. Acoust. Soc. Am. 118, 3447–3456.